IEEE Photonics Journal
An IEEE Photonics Society Publication

Open Access

Efficient Light Trapping in Organic Solar Cell Using a Short-Pitched Hexagonal Array of Metallic Nanocylinders

Volume 8, Number 5, October 2016

Wenyan Wang
Ye Zhang
Ming Chen
Yuying Hao
Ting Ji
Furong Zhu
Yanxia Cui

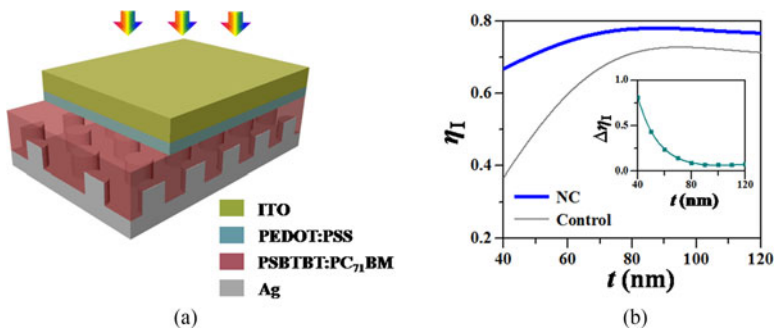

DOI: 10.1109/JPHOT.2016.2614601
1943-0655 © 2016 IEEE

IEEE photonics SOCIETY

IEEE

Efficient Light Trapping in Organic Solar Cell Using a Short-Pitched Hexagonal Array of Metallic Nanocylinders

Wenyan Wang,[1] Ye Zhang,[1] Ming Chen,[1] Yuying Hao,[1] Ting Ji,[1] Furong Zhu,[2] and Yanxia Cui[1]

[1]Key Laboratory of Advanced Transducers and Intelligent Control System of Ministry of Education, College of Physics and Optoelectronics, Taiyuan University of Technology, Taiyuan 030024, China
[2]Department of Physics, Hong Kong Baptist University, Hong Kong

DOI:10.1109/JPHOT.2016.2614601

Manuscript received September 1, 2016; revised September 24, 2016; accepted September 27, 2016. Date of publication September 30, 2016; date of current version October 19, 2016. This work was supported in part by the National Natural Science Foundation of China under Grant 61274056, Grant 61475109, and Grant 61275037; in part by the Key Research and Development (International Co-operation) Program of Shanxi under Grant 201603D421042; and in part by the Platform and Base Special Project of Shanxi under Grant 201605D131038. The work of Y. Cui was supported by the Young Talents Program and Young Sanjin Scholars Program of Shanxi Province and the Outstanding Youth Funding at Taiyuan University of Technology. Corresponding authors: Y. Hao and Y. Cui (e-mail: haoyuying@tyut.edu.cn; yanxiacui@gmail.com).

Abstract: Plasmonic nanostructures have a great potential for enhancing light absorption of organic solar cells (OSCs). Our previous work has demonstrated that light absorption for OSCs with thin active layer can be significantly increased with a 1-D short-pitched metal grating, but the absorption enhancement is sensitive to the polarization of light and vanishes when the active layer is thicker than 60 nm. In this work, we extend the grating into 2-D space, specifically, with metallic nanocylinders packed in a hexagonal array embossed at the silver cathode. Numerical calculations indicate that the proposed OSC not only possesses polarization insensitivity but outperforms the corresponding equivalent planar device as well when the thickness of the active layer changes over a wide range from 40 to 120 nm. The absorption enhancement factor increases with the decrease of the active layer thickness, reaching 81.5% when the active layer is 40-nm thick. The evident enhancement in absorption is mainly due to the excitation of the strong dipole-like surface plasmon resonance, as well as their mutual coupling between neighboring nanocylinders. The present work could provide a promising route for the development of high-efficiency OSCs.

Index Terms: Organic solar cells, absorption enhancement, gratings, surface plasmon.

1. Introduction

Efficient light trapping is greatly desired for organic solar cells (OSCs) to satisfy the requirement that the active layer should be optically thick and electrically thin [1], [2] due to low carrier mobility in organic semiconductors [3]. In the past years, we have witnessed a significant improvement on performance of OSCs using metallic nanostructures [1], [2], [4], [5]. Among them, utilizing the nanostructured metal back reflectors in OSCs is confirmed to be a highly effective route of harvesting light [6]–[21]. The light trapping ability of the metal back reflector is influenced by its shape, dimension, and arrangement of the geometry. In principle, the absorption enhancement

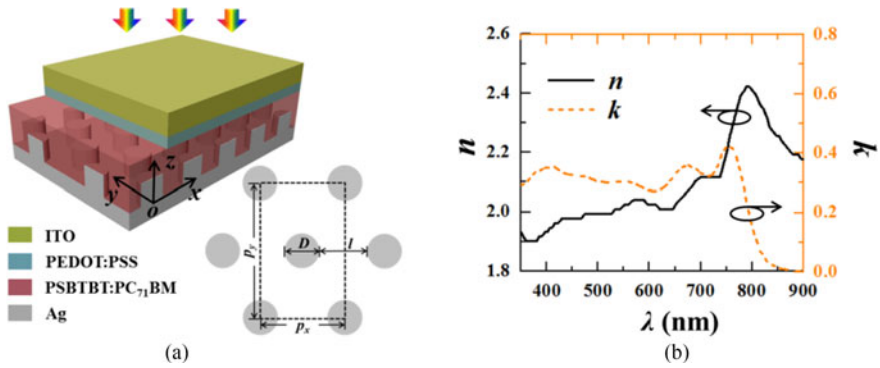

Fig. 1. (a) Therefore, Schematic diagram of the proposed OSCs with patterned back cathode. The subgraph at lower right corner shows the specific hexagonal array of silver nanocylinders patterned in the back cathode. (b) Complex refractive indices of PSBTBT:PC_{71}BM with *n* and *k* representing the real and imaginary parts, respectively.

in the active layer is achieved by the excitations of surface plasmon resonances (SPRs) and/or photonic modes [22]. For 1-D metal grating, SPRs can only be excited under the transverse magnetic (TM) polarized incidence, which means the increase of light absorption impossibly occur at the transverse electric (TE) polarization by SPRs [2], [6]–[13]. One can enhance light absorption at TE polarization by resorting to the excitation of photonic modes [6], [11], [13]. Even though, this kind of OSCs still suffers the polarization sensitivity as the excited optical resonances are different at different polarizations. Instead, if the metal grating is extended into 2-D space, the plasmonic resonances can be independent of the polarization of the incident light, resulting in a further enhancement in absorption in OSCs at hybrid polarization [14]–[21].

It is noted that most of the existing investigations have focused on the metallic nanoarrays having scales larger than a hundred of nanometers [14]–[21], [23]–[26], while those with smaller geometry, being widely applied in surface-enhanced Raman spectroscopy [27], [28], have been rarely explored in the area of OSCs. In our previous works [29]–[31], we have demonstrated the potential of 1-D short-pitched metal gratings in enhancing light absorption of active layer in OSCs. In this paper, a 2-D short-pitched hexagonal array of metal nanocylinders is developed to further improve the light absorption property in OSCs. The proposed plasmonic OSC outperforms the equivalent planar device when the thickness of the active layer changes from 40 nm to 120 nm. Compared to the planar control cell with the active layer at its optimized thickness, our plasmonic OSC demonstrates 7.3% higher integrated absorption. The absorption enhancement factor reaches 81.5% when the thickness of the active layer decreases to 40 nm. Meanwhile, our proposal exhibits the pronounced absorption enhancement at wide angular ranges. In practice, such a 2-D metal grating incorporated OSC can be realized by the nano-imprinting method, and expensive techniques, e.g., the electron beam lithography, can be partly replaced [32]. It is expected that our proposal will provide a promising strategy for developing high efficiency OSCs.

2. Structure and Method

Fig. 1(a) illustrates the 3-D schematic diagram of the proposed OSC with a hexagonal array of silver nanocylinders introduced at the back cathode. The top ITO layer as the transparent conductive anode has a thickness of 100 nm. The adjacent planar PEDOT:PSS is 20 nm thick as the hole transporting layer. The following patterned PSBTBT:PC_{71}BM (consisting of the blend of poly{(4,4'-bis(2-ethylhexyl)dithieno(3, 2-b; 2', 3'-d)silole)-2, 6 -diyl-alt-(2, 1, 3- benzothiadiazole)-4, 7-diyl} and [6, 6]-phenyl C71-betyric acid methyl ester) is used as the active layer with a thickness of *t*. The back cathode is a continuous Ag film of 200 nm thick combined with a hexagonal array of silver nanocylinders with height of *h* deeply embedded into the active layer, which simultaneously performs as a plasmonic coupler to achieve light trapping. The geometry of the

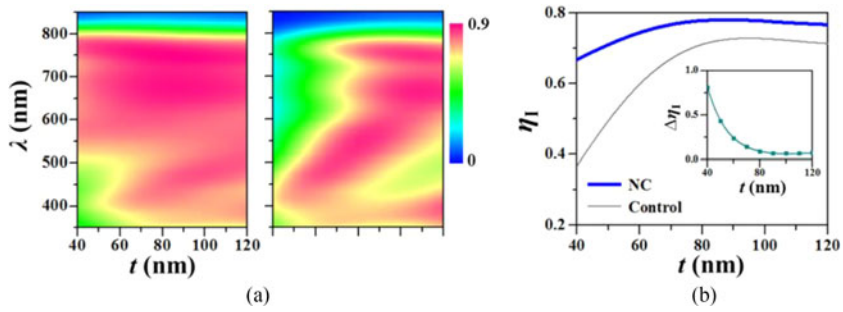

Fig. 2. (a) Maps of the absorption of the active layer versus its thickness and incident wavelength for the NC device (left) and the equivalent planar control device (right). (b) Integrated absorption efficiency in the active layer (η_l) as a function of the thickness of active layer (t) for the NC device and the equivalent planar control device with the inset displaying the corresponding enhancement factors ($\Delta\eta_l$).

hexagonal array of silver nanocylinders is displayed in the subgraph of lower right corner of Fig. 1(a), in which D represent the diameter of cylinders, and $l + D/2$ indicates the distance between the centers of two adjacent cylinders. In the simulated unit cell [see the dotted box shown in Fig. 1(a)], p_x and p_y are the periods of the hexagonal array along x-axis and y-axis directions, equal to $D + l$ and $\sqrt{3}p_x$, respectively. The fill factor f is defined as D/p_x.

The proposed OSC are investigated theoretically by the Finite Difference Time Domain (FDTD) method [33], which has been verified by repeating the work in [17] and [34]. All simulations are carried out with periodic boundary conditions applied along both x-axis and y-axis, and perfectly matched layer (PML) boundaries along z-axis. Light are illuminated from the top ITO side at TM (or TE) polarization, which has the magnetic component (or the electric component) along the y-axis. The wavelength dependent refractive indices (n) of PSBTBT:$PC_{71}BM$ are obtained from [35]; see Fig. 1(c). In addition, other refractive indices related in this work are extracted from [29]–[31]. The absorption efficiency (η) and integrated absorption efficiency (η_l) of the active layer are calculated over the wavelength range from 350 nm to 850 nm. In addition, the planar cell is also investigated as the control, of which the active layer has an equivalent thickness as that of the proposed cell (denoted as NC) for ensuring the same volume of active material in both structures. The optimized parameters of nanocylinders are $l = 12$ nm, $D = 12$ nm, and $h = 35$ nm according to our calculations.

3. Results and Discussions

Fig. 2(a) shows the maps of light absorption in the active layer as a function of the active layer thickness (t) and incident wavelength (λ) under normal incidence for the NC device with optimized nanocylinders (left) and the equivalent control device (right). The integrated absorption efficiencies (η_l) of the active layer versus t for both the NC and control devices are shown in Fig. 2(b). The inset in Fig. 2(b) shows the enhancement factors of the integrated absorption efficiency for the NC device with respect to the equivalent control device [$\Delta\eta_l$, calculated by $(\eta_{l\_NC} - \eta_{l\_Control})/\eta_{l\_Control}$] at different thicknesses of the active layer. It can be seen clearly from Fig. 2(b) that the absorption performance of the NC device is always superior to that of the control device when t is tuned from 40 nm to 120 nm. At the cases with small t, the absorption of the planar cell is quite poor, especially at wavelengths longer than 500 nm; the corresponding η_l of the equivalent planar cell when $t = 40$ nm (corresponding to an equivalent thickness of 32 nm in planar cell) is only 36.8%. With the increase of t, the absorption of the equivalent planar cell becomes increasingly higher until $t = 93$ nm (corresponding to an equivalent thickness of 85 nm in planar cell), and the maximum η_l of 72.9% is achieved, in which the first order Fabry-Perot (FP) cavity resonance is excited with efficient absorption produced at the wavelength range between 500 nm and 800 nm. Against the planar cell is that fact that the plasmonic OSC including the hexagonal array of silver nanocylinders displays very efficient absorption even when the active layer is very thin. We see in Fig. 2(a)

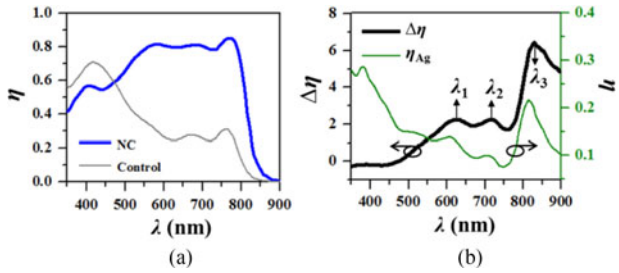

Fig. 3. (a) Absorption spectra in the active layer for the NC device (thick) and the equivalent planar control device (thin). (b) (Thick) Absorption enhancement spectrum ($\Delta\eta$) of the NC device relative to the equivalent control device with three enhancement peaks as labeled $\lambda_1 = 630$ nm, $\lambda_2 = 718$ nm, and $\lambda_3 = 828$ nm. (Thin) Absorption spectrum in the Ag cathode with the hexagonal array of nanocylinders for the NC device.

that when $t = 40$ nm, the NC device performs outstanding absorption at the wavelength range between 500 nm and 800 nm, and the corresponding η_I is 66.8%, reaching 91.6% of the highest η_I (72.9%) of the planar device and increased by 81.5% (88% under AM 1.5G solar spectrum illumination) with respect to that of the equivalent planar control device. Such a desirable η_I of the NC device with only 40 nm thick structured active layer is equal to that of the planar device with about 62 nm thick active layer, which means a large reduction in material consumption achieved by our proposal. As t increases from 40 nm to 120 nm, the integrated absorption of the NC device first increases then reaches the stable status. With the increase of t, the enhancement factor [the insert of Fig. 2(b)] first decreases then getting to the stable status of ~8%. For the NC device, the maximum η_I is 78.2% achieved at $t = 85$ nm, exceeding the maximum η_I for the planar device by 7.3% (6.8% under AM 1.5G solar spectrum illumination). The above investigations indicate that our proposed structure is more efficient for improving light harvesting in a thinner active layer. In consideration of electrical properties of OSCs, thin active layer should also be more beneficial to provide a short charge transport path for minimizing the bulk recombination loss and facilitating charge collection. Therefore, as long as thin active layer can absorb enough incident light by light manipulate structure, it should be approved in a real OSCs. However, the devices with thin active layer maybe suffer from the risk of shunting paths because the formation of non pin-hole homogenous thin active film is very challenging in experimentally.

We further examine the detailed absorption property of the NC device with $t = 40$ nm. Fig. 3(a) shows the absorption spectra of the NC device (thick line) and the equivalent control device (thin line). It is observed that the absorption efficiency η is drastically enhanced over a very wide wavelength range from 474 nm to 900 nm and is slightly decreased in a narrow wavelength range from 350 nm to 474 nm. The absorption enhancement overwhelmingly outperforms the absorption decline, bringing forward a considerable increase in the integrated absorption efficiency η_I [see Fig. 2(b)]. The enhancement factors of absorption over the investigated wavelength range for the NC device compared with the equivalent control device [$\Delta\eta$, calculated by $(\eta_{\text{NC}} - \eta_{\text{Control}})/\eta_{\text{Control}}$] are shown in Fig. 3(b) (thick line). Three significant enhancement peaks are observed at $\lambda_1 = 630$ nm, $\lambda_2 = 718$ nm and $\lambda_3 = 828$ nm with $\Delta\eta$ of 226%, 226% and 643%, respectively. Meanwhile, the absorption spectrum in the Ag cathode containing nanocylinders (η_{Ag}) is also plotted; see Fig. 3(b) (thin line). It is found that at the three enhancement peaks, the absorption in the Ag cathode also reaches its local maxima. It is then deduced that the absorption enhancement in the active layer could be ascribed to the excitation of resonances produced by the Ag nanostructures (as presented in the following). It is also noticed the Ag cathode with nanocylinders possesses a very strong absorption peak at 382 nm, but the absorption of the active layer in the corresponding NC device is suppressed with respect to the planar control. This is because the material property of Ag at this wavelength range is no longer noble metal but lossy dielectric [29]–[31].

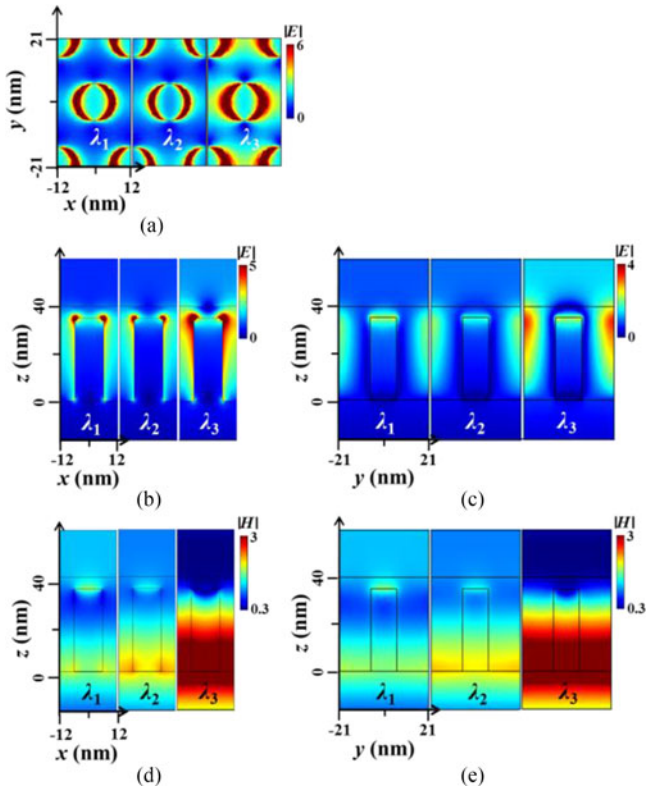

Fig. 4. (a)-(c) Distributions of the electric field intensity $|E|$ in the *x*-*y*, *x*-*z*, and *y*-*z* plane, respectively, (d) and (e) Distributions of the magnetic field intensity $|H|$ in the *x*-*z* and *y*-*z* plane, respectively, at the three labeled enhancement peaks for the proposed structure under TM polarization.

To elucidate the physical origin of the observed absorption enhancement in the proposed NC device, the electromagnetic field distributions at the three enhancement peaks [λ_1, λ_2, and λ_3 as labeled in Fig. 3(b)] are investigated under TM polarization. Here, the distributions of the electric field amplitude ($|E|$) at the x-y plane at the top surface of the nanocylinders, the *x*-*z* plane at $y = 0$ and the *y*-*z* plane at $x = 0$ are plotted in Fig. 4(a)–(c). One sees clearly that, at all three wavelengths, there are very strong electric field accumulated around the Ag nanocylinders, which belongs to the dipole-like localized surface plasmon resonance (D-LSPR) [36]. Mutual coupling of D-LSPRs between neighboring Ag nanocylinders is observed along x axis as well as y axis. Especially, among the three investigated cases, the coupling effect is the strongest at λ_3. Such coupling effect of D-LSPRs is beneficial to the field enhancement in the active material located between neighboring Ag nanocylinders, as we see in Fig. 4(b) and 4(c) that the electric field intensity in-between neighboring Ag nanocylinders is quite stronger at λ_3 than at other two wavelengths. That could be the reason why the enhancement factor of the integrated light absorption at λ_3 is much higher than that at λ_1 or λ_2. It is noticed from Fig. 4(c) that there is also a penetration of light at the head of the Ag nanocylinders due to the excitation of D-LSPRs and their mutual coupling, but it is strange that the amplitude of $|E|$ at the head of Ag nanocylinders does not increase linearly when approaching the wavelength of the strong coupled D-LSPR mode (i.e., λ_3). Here, one sees that the amplitude of $|E|$ at the head of Ag nanocylinders is stronger at λ_1 than at λ_2. To explain that phenomenon, the distributions of the magnetic field amplitude ($|H|$) at the x-z plane at $y = 0$ and the *y*-*z* plane at $x = 0$ are calculated as plotted in Fig. 4(d) and (e). The abnormal change of $|E|$ at the head of Ag nanocylinders could be attributed to the excitation of magnetic resonance. It is observed from Fig. 4(d) and (e) that the accumulation of magnetic field are produced at the head of Ag nanocylinders at λ_1 and λ_2 but not at λ_3. As is well known, at the metal/dielectric interface, propagating

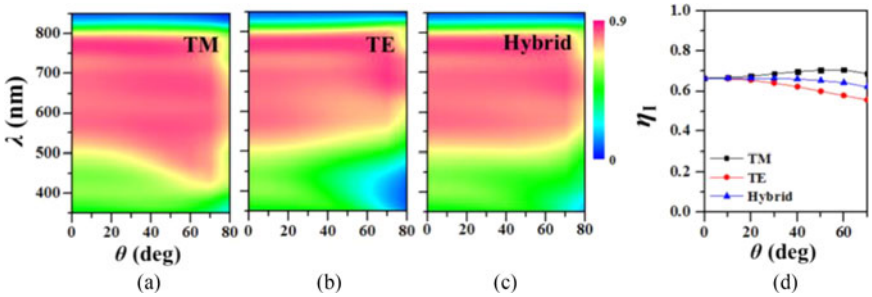

Fig. 5. (a)–(c) Angular dependent absorption maps at different polarizations for the proposed NC device. (d) Integrated absorption efficiency in the active layer (η_I) versus the incident angle θ at different polarizations.

surface plasmon polaritons (SPPs) can be excited [22], [28]. In our design, the top surface of the Ag nanocylinders acts as the metal/dielectric interface exciting propagating SPPs, which gets reflected back and forth when meeting the sidewall of the Ag nanocylinders. The resulted resonant profile is as displayed in Fig. 4(d) and (e). The magnetic field is more stretched at the center of the top surface of the Ag nanocylinders than at the side corner. Obviously, the magnetic field located at the head of the Ag nanocylinders at λ_1 is stronger, correspondingly bringing forward a stronger electric field, than that at λ_2. This can just explain why the $|E|$ amplitude at λ_1 is stronger than that at λ_2. In Fig. 4(d) and (e), uniform magnetic field is also observed at the bottom of active layer ($z = 0$) at all three wavelengths because such a short-pitched grating can be regarded as a planar effective medium with anisotropic permittivities [37]. To sum up, the absorption enhancement induced in our plasmonic OSC device mainly origin from the excitation of D-LSPRs as well as their mutual coupling while the magnetic resonance at the top head of Ag nanocylinders only plays a minor role.

The light absorption performance at off-normal incidence is also an important aspect for OSCs as the angle of the solar radiation changes over time. Fig. 5(a)–(c) show the angular dependent absorption maps in the active layer under different polarized light incidence for the proposed structure when $t = 40$ nm. Fig. 5(d) displays the integrated absorption efficiencies (η_I) versus the incidence angle at different polarizations. As can be seen from Fig. 5(a), at TM polarization, the absorption band is broadened gradually, so that η_I increases from 66.8% to 68.6% as the incident angle changes from 0 to 70 degree. While at TE polarization, the absorption band become narrow gradually [see Fig. 5(b)], bringing forward a roll-off of 16.5% in η_I when the incident angle is tuned from 0 to 70 degree. The distinct angular responses under different polarizations originate from the difference in the direction of the electric field component at different incident angle [38], [39], which mainly affects the intensity of D-LSPR resonance excited. In addition, we found that the magnetic field distributions (not shown here) at oblique incidence perform a relatively stronger cavity resonance compared to the case at normal incidence at short wavelength range from 350 nm to 500 nm [38], which should also be responsible for the enhanced absorption under TM polarization at large incident angles except for the strengthened plasmonic resonant modes. Benefiting from the wide-angle, broad-band, and high-factor absorption enhancement at TM polarization, the designed NC device exhibits an angular insensitive absorption response at TM/TE hybrid polarization; see Fig. 5(c), with only a decrease of 6.6% in η_I as the incident angle increases from 0 to 70°. Such omnidirectional feature is very favorable for practical applications of solar harvesting.

Next, numerical studies on the influences of the geometrical parameters of the Ag nanocylinders on the absorption performance of the NC device are carried out at normal incidence. First, with p_x fixed to 24 nm, we investigate the dependence of η_I on the height (h) and fill factor (f) of the Ag nanocylinders array; see Fig. 6(a). It is observed that both the height and fill factor of the nanocylinders have important influences on η_I. The optimized result of η_I is obtained at $h = 35$ nm and $f = 0.5$, denoted as point A in Fig. 6(a). In detail, the absorption spectra with f tuned (at $h = 35$ nm) or with h tuned (at $f = 0.5$) are investigated, as shown in Fig. 6(b) and 6(c), respectively. One can see from Fig. 6(b) that the light absorption is strengthened in long wavelength band and

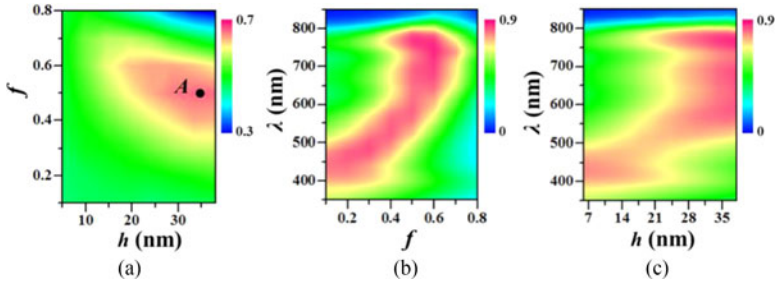

Fig. 6. (a) Map of integrated absorption efficiency in the active layer versus the height (h) and fill factor (f) of the Ag nanocylinders array at normal incidence. Case A represents the point with maximum integrated absorption efficiency, where $h = 35$ nm and $f = 0.5$. (b) and (c) Absorption spectra when the fill factor f and the height h of nanocylinders are tuned, respectively.

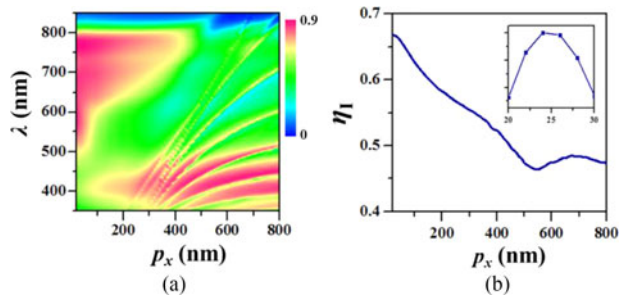

Fig. 7. (a) Absorption spectra as a function of the period (p_x) of the nanocylinder array at normal incidence. (b) Integrated absorption efficiency versus p_x.

is weakened in short wavelength band with the increase of f. The careful investigations of field distributions indicate that the variation of f does not induce any new light capturing mechanisms but only impacts on the strength of resonant modes. The larger, f the more the energy loss in the Ag nanocylinders, resulting in the decline of light absorption in the short wavelength band. The smaller f the weaker the coupling of D-LSPRs between neighboring Ag nanocylinders, bringing forward the decrease of light absorption in the long wavelength band. The strongest light absorption is gained when f is equal to 0.5. Similarly, it can be seen from Fig. 6(c) that as h increases gradually, the light absorption becomes stronger in the long wavelength band. Obviously, this is because short nanocylinders are inferior to generate D-LSPRs than long nanocylinders. Here, since the thickness of the active layer is fixed, the increase of the nanocylinders height brings the reduction of the volume of the active material. As a result, the integrated absorption efficiency is maximized at $h = 35$ nm.

Finally, the influence of the period of the nanocylinder array (p_x) on the light absorption of the active layer in NC devices is investigated. Fig. 7(a) displays the absorption spectra at tuned p_x. The optimized parameters of h and f ($h = 35$ nm and $f = 0.5$) are used in calculation. Obviously, it is observed from Fig. 7(a) that the absorption band of the active layer is wider and the related absorption efficiency is stronger when p_x is smaller than ~80 nm. As p_x increases, the absorption band becomes significantly weakened in the long wavelength region as the D-LSPRs are less efficiently excited. It is noticed that, as p_x is greater than 100 nm, there is an absorption band centered at about 400 nm, which is actually the same absorption band as that observed in the spectrum of the planar OSC [as shown in the right panel of Fig. 2(b) $t = 40$ nm, as well as in Fig. 3(a), the thin line] because the nanocylinders take only a quite small part of the whole period. This band suffers serious mode splitting when p_x becomes greater than 200 nm, due to the optical lattice scattering effect of the nanocylinder array. Furthermore, the integrated absorption efficiency (η_I) versus the array period (p_x) is calculated, as shown in Fig. 7(b). It is found that with the increase of p_x, η_I gradually drops and reaches its minimum value of 46.3% at $p_x = 550$ nm, nevertheless,

still superior over that of the planar cell (36.8% with $t = 40$ nm). With the further increase of p_x, another local maximum of η_l (48.5%) is produced at $p_x = 670$ nm but much lower than that when $p_x = 24$ nm (the structural parameter used in our design). The plasmonic grating with relatively large period should be further optimized before being applied in the present OSC structure and related studies can be found in [18] and [19].

4. Conclusion

In conclusion, an OSC based on a silver cathode possessed with a hexagonal array of nanocylinders has been explored numerically for improving the light trapping ability in the active layer. Our study reveals that the utilization of such a 2-D nanostructured Ag cathode outstandingly improves the absorption in the active layer relative to the planar control device, when the thickness of the active layer changes from 40 nm to 120 nm. The integrated absorption efficiency for the OSC with a 40 nm-thick active layer under un-polarized normal incidence reaches 66.8%, equal to that of the planar device with about 62 nm thick active layer, saving approximately half of the active material. Particularly, the maximum integrated absorption efficiency of the NC device is 78.2% increased by 7.3% over that of the planar device. The improved light trapping behavior for our proposed device is mainly attributed to the excitation of D-LSPR mode and the strong coupling of D-LSPR modes between neighboring Ag nanocylinders. In addition, our proposal demonstrates a wide angular and polarization-insensitive absorption property. The dependences of absorption properties on the geometrical parameters have also been studied. The proposed design is expected to provide a promising route for the development of high-efficiency OSCs.

References

[1] H. A. Atwater and A. Polman, "Plasmonics for improved photovoltaic devices," *Nature Mater.*, vol. 9, no. 3, pp. 205–213, 2010.
[2] Q. Gan, F. J. Bartoli, and Z. H. Kafafi, "Plasmonic-enhanced organic photovoltaics: Breaking the 10% efficiency barrier," *Adv. Mater.*, vol. 25, no. 17, pp. 2385–2396, 2013.
[3] P. W. Blom, V. D. Mihailetchi, L. J. A. Koster, and D. E. Markov, "Device physics of polymer: Fullerene bulk heterojunction solar cells," *Adv. Mater.*, vol. 19, no. 12, pp. 1551–1566, 2007.
[4] W. C. H. Choy, "The emerging multiple metal nanostructures for enhancing the light trapping of thin film organic photovoltaic cells," *Chem. Commun.*, vol. 50, no. 81, pp. 11967–12206, 2014.
[5] X. G. Ren *et al.*, "High efficiency organic solar cells achieved by the simultaneous plasmon-optical and plasmon electrical effects from plasmonic asymmetric modes of gold nanostars," *Small*, vol. 12, pp. 5200–5207, doi: 10.1002/smll.201601949, 2016.
[6] X. H. Li *et al.*, "Dual plasmonic nanostructures for high performance inverted organic solar cells," *Adv. Mater.*, vol. 24, no. 22, pp. 3046–3052, 2012.
[7] R. B. Dunbar, T. Pfadler, and L. Schmidt-Mende, "Highly absorbing solar cells—A survey of plasmonic nanostructures," *Opt. Exp.*, vol. 20, no. 102, pp. A177–A189, 2012.
[8] X. H. Li, W. E. I. Sha, W.C. H. Choy, D. D. Fung, and F. X. Xie, "Efficient inverted polymer solar cells with directly patterned active layer and silver back grating," *J. Phys. Chem. C*, vol. 116, no. 12, pp. 7200–7206, 2012.
[9] M. A. Sefunc, A. K. Okyay, and H. V. Demir, "Plasmonic backcontact grating for P3HT: PCBM organic solar cells enabling strong optical absorption increased in all polarizations," *Opt. Exp.*, vol. 19, no. 15, pp. 14200–14209, 2011.
[10] M. Yousefi and A. Alighanbari, "Random plasmonic nanowire gratings for enhanced light absorption in organic solar cells," *Plasmonics*, vol. 10, no. 6, pp. 1751–1759, 2015.
[11] A. Baba, N. Aoki, K. Shinbo, K. Kato, and F. Kaneko, "Grating-coupled surface plasmon enhanced short-circuit current in organic thin-film photovoltaic cells," *ACS Appl. Mater. Interfaces*, vol. 3, no. 6, pp. 2080–2084, 2011.
[12] E. Wei, W. C. H. Choy, and W. C. Chew, "Angular response of thin-film organic solar cells with periodic metal back nanostrips," *Opt. Lett.*, vol. 36, no. 4, pp. 478–480, 2011.
[13] X. M. Tian *et al.*, "Omnidirectional and polarization-insensitive light absorption enhancement in an organic photovoltaic device using a one-dimensional nanograting," *J. Modern Opt.*, vol. 61, no. 21, pp. 1714–1722, 2014.
[14] S. In and N. Park, "Inverted ultrathin organic solar cells with a quasi-grating structure for efficient carrier collection and dip-less visible optical absorption," *Sci. Rep.*, vol. 6, no. 21784, pp. 1–7, 2016.
[15] S. In, D. R. Mason, H. Lee, M. Jung, C. Lee, and N. Park, "Enhanced light trapping and power conversion efficiency in ultrathin plasmonic organic solar cells: a coupled optical-electrical multiphysics study on the effect of nanoparticle geometry," *ACS Photon.*, vol. 2, no. 1, pp. 78–85, 2014.
[16] K. Q. Le, "Broadband and polarization-insensitive solar absorption enhancement in thin-film organic solar cells using metallic nanopillars," *IEEE J. Photovolt.*, vol. 4, no. 6, pp. 1566–1569, Nov. 2014.
[17] W. Bai, Q. Gan, G. Song, L. Chen, Z. Kafafi, and F. Bartoli, "Broadband short-range surface plasmon structures for absorption enhancement in organic photovoltaics," *Opt. Exp.*, vol. 18, no. 104, pp. A620–A630, 2010.

[18] A. Fallahpour, G. Ulisse, M. Auf der Maur, A. Di Carlo, and F. Brunetti, "3-D simulation and optimization of organic solar cell With periodic back contact grating electrode," *IEEE J. Photovolt.*, vol. 5, no. 2, pp. 591–596, Mar. 2015.
[19] X. Li, W. C. Choy, X. Ren, J. Xin, P. Lin, and D. C. Leung, "Polarization-independent efficiency enhancement of organic solar cells by using 3-dimensional plasmonic electrode," *Appl. Phys. Lett.*, vol. 102, no. 15, 2013, Art. no. 153304.
[20] W.-F. Xu, M.-Y. Pan, P.-H. Fu, S.-W. Li, D.-W. Huang, and P.-K. Wei, "Efficiency enhancement of top-illuminated ITO-free organic solar cells using plasmonic-assisted nanostructured reflective electrodes," *J. Mater. Chem. C*, vol. 3, no. 35, pp. 9131–9136, 2015.
[21] Y.-G. Bi *et al.*, "Dual-periodic-corrugation-induced broadband light absorption enhancement in organic solar cells," *Org. Electron.*, vol. 27, pp. 167–172, 2015.
[22] Y. Cui *et al.*, "Plasmonic and metamaterial structures as electromagnetic sbsorbers," *Laser Photon. Rev.*, vol. 8, no. 4, pp. 495–520, 2014.
[23] E. Lee and C. Kim, "Analysis and optimization of surface plasmon-enhanced organic solar cells with a metallic crossed grating electrode," *Opt. Exp.*, vol. 20, no. 105, pp. A740–A753, 2012.
[24] Q. G. Du *et al.*, "Light absorption mechanism in organic solar cells with hexagonal lattice nanohole aluminum transparent electrodes," *J. Opt.*, vol. 17, no. 8, 2015, Art. no. 085901.
[25] C. J. An *et al.*, "Surface plasmon assisted high performance top-illuminated polymer solar cells with nanostructured Ag rear electrodes," *J. Mater. Chem. A*, vol. 2, no. 9, pp. 2915–2921, 2014.
[26] K. Aydin, V. E. Ferry, R. M. Briggs, and H. A. Atwater, "Broadband polarization-independent resonant light absorption using ultrathin plasmonic super absorbers," *Nature Commun.*, vol. 2, no. 517, pp. 1–7, 2011.
[27] Z. Zhou *et al.*, "From 1D to 3D: Tunable sub-10 nm gaps in large area devices," *Adv. Mater.*, vol. 28, no. 15, pp. 2956–2963, 2016.
[28] Z. Huang *et al.*, "Surface-enhanced raman scattering from Au-nanorod arrays with sub-5-nm gaps stuck out of an AAO template," *J. Nanosci. Nanotechnol.*, vol. 16, no. 1, pp. 934–938, 2016.
[29] W. Wang *et al.*, "High-efficiency, broad-band and wide-angle optical absorption in ultra-thin organic photovoltaic devices," *Opt. Exp.*, vol. 22, no. 102, pp. A376–A385, 2014.
[30] Y. Zhang *et al.*, "Absorption enhancement in organic solar cells with a built-in short-pitch plasmonic grating," *Plasmonics*, vol. 10, no. 4, pp. 773–781, 2015.
[31] W. Wang *et al.*, "Ultra-thin organic solar cells incorporating dielectric-coated comb silver nanogratings," *Plasmonics*, vol. 11, no. 1, pp. 151–157, 2016.
[32] Z. Yong-Jun *et al.*, "Fabrication of nanoimprint mold by multilayer film deposition technique," *Acta Phys. Sin.*, vol. 55, no. 4, pp. 2033–2037, 2006.
[33] A. Tavlove, *Computational Electrodynamics: The Finite-Difference Time Domain Method*. Norwood, MA, USA: Artech House, 1995.
[34] D. Duche, P Torchio, L. Escoubas, F. Monestier, J. J. Simon, and F. Flory, "Improving light absorption in organic solar cells by plasmonic contribution," *Sol. Energy Mater. Solar Cells*, vol. 93, no. 8, pp. 1377–1382, 2009.
[35] J. Mescher *et al.*, "Design rules for semi-transparent organic tandem solar cells for window integration," *Org. Electron.*, vol. 15, no. 7, pp. 1476–1480, 2014.
[36] S. A. Maier, *Plasmonics: Fundamentals and Applications*. New York, NY, USA: Springer, 2007.
[37] Y. Cui *et al.*, "Ultrabroadband light absorption by a sawtooth anisotropic metamaterial slab," *Nano Lett.*, vol. 13, no. 3, pp. 1443–1447, 2012.
[38] K. Liu *et al.*, "Wide-Angle and polarization-insensitive perfect absorber for organic photovoltaic layers," *IEEE Photon. Technol. Lett.*, vol. 25, no. 13, pp. 1266–1269, Jul. 2013.
[39] X. G. Ren, X. C. Li, and W. C. H. Choy, "Optically enhanced semi-transparent organic solar cells through hybrid metal/nanoparticle/dielectric nanostructure," *Nano Energy*, vol. 17, pp. 187–195, 2015.